AD-A051 299 NAVAL RESEARCH LAB WASHINGTON D C F/G 21/5
NUMERICAL PARAMETRIC STRESS ANALYSIS OF THE TF-30 TURBINE ENGIN--ETC(U)
JAN 78 L A BEAUBIEN

UNCLASSIFIED NRL-MR-3671 SBIE-AD-E000 121 NL

| OF |
AD
A051 299

END
DATE
FILMED
4-78
DDC

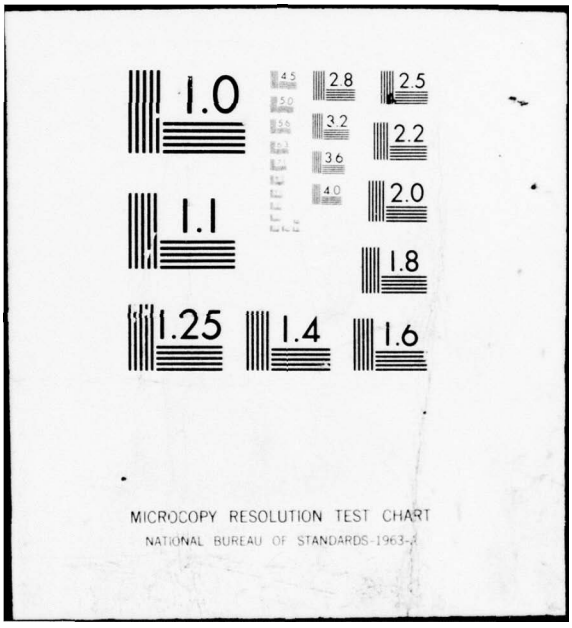
1.0
1.1
1.25
1.4
1.6
1.8
2.0
2.2
2.5
2.8
3.2
3.6
4.0
4.5
5.0
5.6
6.3
7.1
MICROCOPY RESOLUTION TEST CHART
NATIONAL BUREAU OF STANDARDS-1963-A

NRL Memorandum Report 3671

Numerical Parametric Stress Analysis of the TF-30 Turbine Engine Third-Stage Fan-Blade/Disk Dovetail Region

L. A. BEAUBIEN

Mechanics of Materials Branch
Ocean Technology Division

January 1978

NAVAL RESEARCH LABORATORY
Washington, D.C.

(18) SBIE (19) AD-E000 121

SECURITY CLASSIFICATION OF THIS PAGE (When Data Entered)

REPORT DOCUMENTATION PAGE

(19) READ INSTRUCTIONS BEFORE COMPLETING FORM

1. REPORT NUMBER: NRL Memorandum Report 3671 — NRL-MR-3671
2. GOVT ACCESSION NO. [redacted]
3. RECIPIENT'S CATALOG NUMBER: Final rept.

(6) 4. TITLE (and Subtitle): NUMERICAL PARAMETRIC STRESS ANALYSIS OF THE TF-30 TURBINE ENGINE THIRD-STAGE FAN-BLADE/DISK DOVETAIL REGION

5. TYPE OF REPORT & PERIOD COVERED: Final report on one phase of a continuing NAVAIR problem.

6. PERFORMING ORG. REPORT NUMBER

(10) 7. AUTHOR(s): L. A. Beaubien

8. CONTRACT OR GRANT NUMBER(s)

9. PERFORMING ORGANIZATION NAME AND ADDRESS: Naval Research Laboratory, Washington, D. C. 20375

10. PROGRAM ELEMENT, PROJECT, TASK AREA & WORK UNIT NUMBERS: NRL Problem F01-30, ~~A5365360-0582~~

(11) 11. CONTROLLING OFFICE NAME AND ADDRESS: Department of the Navy, Naval Air Systems Command, Washington, D. C. 20361

12. REPORT DATE: Jan[redacted]78

13. NUMBER OF PAGES: ~~35~~ (13) 36 pp.

14. MONITORING AGENCY NAME & ADDRESS (if different from Controlling Office)

15. SECURITY CLASS. (of this report): UNCLASSIFIED

15a. DECLASSIFICATION/DOWNGRADING SCHEDULE

16. DISTRIBUTION STATEMENT (of this Report): Approved for public release; distribution unlimited.

17. DISTRIBUTION STATEMENT (of the abstract entered in Block 20, if different from Report)

18. SUPPLEMENTARY NOTES

19. KEY WORDS (Continue on reverse side if necessary and identify by block number)

Stress analysis
Turbine engine
Finite element

20. ABSTRACT (Continue on reverse side if necessary and identify by block number)

A two-dimensional finite element parametric analysis was conducted for the disk/blade dovetail region of the TF-30 turbine engine, assuming purely radial (centrifugal) loading of the blade. A graphical boundary matching procedure was used to determine a likely disk/blade interface force distribution. This distribution produced a stress concentration factor (SCF) of 5.3 in the disk fillet, relative to the average stress in the neck section of the disk. In addition, the SCF was found to decrease with decreasing interface friction. Parametric modification of the disk fillet resulted in a maximum SCF reduction of 27%, achieved with a fillet radius of three

→ over (Continues)

251 950

20. Abstract (Continued)

times the present one. For all studied combinations of interface force distribution, coefficient of friction and fillet geometry the point of maximum tensile stress occurred farther into the fillet (away from the contact region) than the point at which cracks appear to initiate (near, or just into the inboard edge of the contact area). However, different combinations of interface force and fillet geometry result in different degrees of spread of the tensile stress concentration from the fillet area into the contact area. Finally, the effects of some assumed interface force perturbations due to non-radial (non-centrifugal) loading are discussed.

CONTENTS

NUMERICAL PARAMETRIC STRESS ANALYSIS OF THE TF-30 TURBINE ENGINE THIRD-STAGE FAN-BLADE/DISK DOVETAIL REGION

1. INTRODUCTION

This report details the numerical portion of a combined experimental/numerical study of the stresses in the third stage fan-blade/disk assembly of the TF-30 turbojet engine used in the F14 aircraft (see Fig. 1). A discussion of the background for this study, as brought on by crack-induced in-service failures of the TF-30 engine, can be found in NRL Report 8149, which contains the results of the experimental program [1]. The experimental study of both the disk and blades involved their response to a single interface loading condition, as produced by an axial (radial) load applied to the blades in the test setup of Fig. 2. The numerical studies reported here were concentrated on the disk/lug contact/fillet area, and involved the sensitivity of this region of the lug to a variation of interface loading parameters such as contact force distribution and normal-force/shear(friction)-force ratios.

2. SIMULATION SYSTEM DESCRIPTION

The parametric finite element analysis was performed using a newly developed interactive, graphics-oriented package called the Two-dimensional Orthotropic Real-Time Analysis Library (TOTAL) [2]. It consists of a set of modular programs linked by a broadly structured disk-file data base. Each of the thirty programs implements a specific task in the simulation/solution/interpretation procedure, and creates data files to be used as needed by other programs further along the solution path. All of the programs are auto-prompting and to a considerable extent auto-instructional with all of the intricacies of data file manipulation hidden from the user. The use of modular programs is intended to encourage numerical experimentation (or parametric analysis). For example, complete or partial changes in files containing boundary conditions, material properties or geometric information can be quickly made by programs made to perform specific modification tasks.

Note: Manuscript submitted December 1, 1977.

The problem can then be resolved without reentering those quantities which did not change. Similarly, compatible result files can be linearly combined to study the effect of superposed solutions. These features were utilized extensively in this study.

3. GENERAL SOLUTION PROCEDURE

The primary mode of failure for the third stage of the TF-30 engine has been observed to be a fracture in the disk-lug contact/fillet area, with some similar but less frequent fracture of the blade. Therefore, the numerical simulation portion of the TF-30 stress analysis concentrated on the lug area by attempting to answer the following three questions.

1. What are the most likely, and most extreme, contact loading conditions expected at the blade/lug interface?

2. What are the maximum values, and distribution characteristics, of the tensile stress field in the contact/fillet areas of the present disk-lug configuration, when subjected to the above loadings?

3. Are there minor geometric modifications which will decrease the tensile stresses?

The program of studies chosen to answer these questions consisted of the following steps.

1. Choice of suitable general geometry and boundary conditions for the various numerical models to be used, based on radial (centrifugal) loading of the blade.

2. Preliminary analysis of coarse-mesh blade and lug models, loaded separately and also in a linked (welded along contact surface) condition.

3. Study of the effect of distribution of interface forces, and of the relative mix of normal and shear (friction) forces.

4. Choice of the most likely distribution of interface forces based on the compatibility of interface displacements for various assumed force distributions.

5. Study of the effect of fillet geometry modification in the lug using a refined mesh and a reference interface loading.

4. GENERAL MODEL CHARACTERISTICS

Basic Geometries

Due to the relatively small angle (5°) between blade and lug center lines, and also the restriction to rectangular cartesian constraints with the TOTAL system, a rectangular (X-Y) modeling was chosen, rather than a cylindrical (R-θ) one. The region to be modeled, taking advantage of symmetry along the center lines of both blade and lug, is illustrated in Fig. 2. The choice of a rectangular modeling had the added advantage of providing for comparison with the results of the experimental photoelastic analysis. The setup for the experimental analysis is shown in Fig. 3. In order to facilitate comparison, the boundaries of the numerical model were taken directly from the working drawings of the photoelastic model, except for the elimination of excess material at the top of the blade and bottom of the lug. The effect of shortening the base of the lug is shown to be negligible later.

The mesh of Fig. 4a is relatively coarse, and was used primarily for the solution of the two parts in a linked condition, and for the few individual solutions run for the blade. For the more extensive studies of the lug, the refined mesh of Fig. 5a was used.

Reference Boundary Conditions

Applied load: The assumed physical loading is a vertical (radial) force applied to the blade, as in the experimental setup of Fig. 3. This loading is assumed to produce identical force distributions on all contact surfaces. (The effect of non-radial loading components is briefly discussed in the Appendix). For the reference loading at the interface of each part, the following force systems, each uniformly distributed, were chosen:

1. A uniformly distributed unit normal force, applied at the seven nodes defining the interface.

2. A .175 (coefficient of friction) distributed shear force, applied at the same seven nodes. (Choice of this friction coefficient is based on initial interpretation of the photoelastic analysis, and on previous numerical analyses of similar configurations. Later analysis of experimental data indicated a friction coefficient of .12 to .16).

Note: for comparison purposes results for all loading cases and geometries are normalized with respect to the combined vertical (Y) component of this reference loading.

Constraints: For the lug, the left and right vertical edges were fixed in the X-direction and free in Y, by invoking free in symmetry conditions. The bottom edge was fixed in Y and X as a first approximation to the condition in the real part and in the photoelastic model. For the blade, the vertical edges were similarly fixed in X, and the top edge was constrained in Y.

Linked condition: For the solution of the two parts linked at the interface, the X-constraint on the vertical edges and the Y-constraint on the bottom edge is maintained, and a uniform distributed Y-force is applied to the top edge of the blade. (See Fig. 3).

5. PRELIMINARY ANALYSIS AND MODEL EVALUATION

Note: Although the quantity of principal interest in this study is the tensile stress, comparisons of various models in this section are made on the basis of isochromatic (maximum shear) patterns, since they afford an immediate comparison with photoelastic results. In addition some isopachic (contours of summed normal stresses, $\sigma_1 + \sigma_2$) fringes are also plotted for comparison with holographic patterns. At a free boundary both of these patterns reduce to the tangential stress.

The results of this section are best presented by discussing Figs. 4 and 5. In Fig. 4a-c the overall maximum shear pattern is shown and also a local enlargement in the critical area (with fringe numbers) for the coarse lug model with the combined reference loading and constraints. The resulting stress concentration factor (SCF) is 4.8.

If the same reference boundary conditions are applied to the refined lug model, Figs. 5b-c show that the general characteristics of the shear pattern do not change, but that there is some change in the critical area (approximately 1/2 fringe) due to the greater resolution. The SCF increases 8% to 5.2.

Figs. 6a-b are a similar representation of what happens if the base of the unrefined model, with the reference loading, is extended in a manner similar to the photoelastic model. It is seen that there is little effective change, and none in the critical region.

The last perturbation on the basic model is illustrated in Figs. 7a-b. The reference interface loading of the refined mesh is maintained, but the right vertical edge is now fixed in both X and Y. Again, although there is some considerable change of the shear pattern near the right edge, the critical area remains unchanged.

For comparison purposes, the photoelastic isochromatic and isopachic fringe patterns are shown in Figs. 8 and 9. Also the numerical isopachic patterns for the reference loading of the coarse and fine lug models are given in Figs. 10a and 10b.

As a final task in the preliminary analysis, the combined blade/lug configuration of Fig. 2 was loaded as described above, and the properly normalized shear contours plotted in Figs. 11a-b. For the combined geometry, and for the critical area of the lug, it is seen that this physically unrealizable case has global features similar to the preceding cases. However, the critical areas for both the blade and the lug are so close to the interface that this linked condition cannot be expected to produce a stress concentration similar to that of the two parts loaded simultaneously and in contact.

The overall conclusions to be drawn from these preliminary investigations are that the refined mesh provides enough improvement over the coarse one to justify the small extra computation cost, that a deep lug base is not required, and that the vertical edges are best left free in Y but fixed in X.

6. INTERFACE FORCE VARIATION

In order to study the effect of location and distribution of the interface forces on the magnitude of the stress concentration in the lug, a series of fourteen distributed and concentrated loadings were applied to the contact surface of the refined lug model. Seven normal loadings, each with a resultant force equal to that of the reference normal loading, are shown in Fig. 12. The other seven loadings consisted of corresponding shear forces with the same distribution and location as the illustrated normal loadings. The total resultant shear force in each case was equal to that of the reference shear loading, or equivalently 17.5% of the corresponding normal force. It should be mentioned here that single point forces are included not as likely physical situations, but simply as hypothetical extreme bounds on the parametric analysis.

For ease in interpretation of results, the following procedure has been used in naming the loading cases. The first character denotes normal (N), shear (S) or combined (NS) loading. The second character denotes distributed (D) or concentrated (C). The third character denotes location of the force resultant at, or near, the bottom (B), middle (M) or top (T) of the contact surface (or combinations of B, M, T).

The results of this parametric analysis are presented in the table of Fig. 12, which contains the SCF for each of the fourteen loads, and also for the combination of corresponding normal and shear loads. In each case, the SCF is obtained by dividing the maximum fillet tensile stress by the average tensile stress across the minimum section connecting the fillet area with the right hand vertical edge.

Effect of distribution

The following trends are evident from a study of Fig. 12. As the centroid of force distribution at the lug interface shifts from the bottom towards the top end, the normal concentration increases but the shear concentration decreases. However, for the assumed reference loading ratio (1.0 normal to .175 shear) the combined stress concentration increases. The overall concentration is bounded by a value of 6.0 for a concentrated load at the top of the interface, as compared to 5.2 for the reference uniformly distributed loading (NDM + SDM).

Effect of friction

For any two corresponding normal and shear loadings (e.g., NDB, SDB), the effect of changing the friction coefficient f, while maintaining the total vertical force constant, can be found by substituting values from the table into the following formula:

$$SCF = \left(\frac{f}{.175}\right) SCFS + \left[1 + (.175 - f)\right] SCFN$$

where SCFS and SCFN are the shear and normal values from the table of Fig. 2. As an example, for loadings NDB and SDB, and for half the reference friction (f = .0825), we get SCF = 4.8. It is seen from the form of the above formula, and from the table values, that a lower coefficient of friction always results in a lower stress concentration.

7. COMPATIBILITY OF INTERFACE FORCES

The following procedure was followed in estimating the most likely interface distribution from among the four distributed load cases of Fig. 12. It is based on the assumption that the true interface distribution should produce, in both the blade and the lug, at least the following two features:

1. The same rotation of the interface surfaces.

2. Maintenance of contact along the interface consistent with the assumed interface loading distribution. For example, loadings concentrated midway along the

interface, and producing a resulting concavity of both surfaces, would be inconsistent.

Since the nature of the chosen interface loading variations (linear variation only) could not be expected to produce the exact interface distribution, a method of simple visual comparison of the approximate compatibility between displaced interfaces of the blade and lug was used. In addition, the solutions for the blade were obtained using the coarse mesh of Fig. 2, whereas the refined model of Fig. 5 was used for the lug. It was not felt that determination of the blade displacements warranted a refined modeling.

As an initial reference, an attempt was made to match the contact surfaces of the distorted geometries of the two parts for the reference uniformly distributed loading. It is seen from Fig. 13a that the difference in interface rotation makes it impossible to match the two end points, and that there is an inadmissable concavity of both surfaces.

Next the assumption was made that contact stresses were concentrated towards the lower end (loading case NDB + SDS). The distorted geometries resulting from this loading are shown in Fig. 13b. It is seen that this results in a much smaller rotational incompatibility, but that the concave curvature is still present along both surfaces.

Next, contact loading concentrated near the upper end (NDT + SDT) as used, and Fig. 13c shows the resulting overlayed surfaces. Here an extreme overlapping at the opposite (lower) end, together with a concave interface curvature, is observed.

These results indicate that any loading spanning the midpoint of the contact surface produces an inadmissable concavity, and that contact stresses should be distributed more towards the lug-fillet end of the interface. This suggests the use of a loading which is zero at the center of the interface, and which varies linearly towards each end, with a greater intensity at the lug-fillet end as in loading case NLIK in Fig. 12. The overlayed displacements are shown in Fig. 13d for a 1.3 to 0.7 ratio of the intensities at the two ends of the contact area. It is seen that the concavity has practically disappeared, while the rotation of the two surfaces remains approximately equal. The conclusion to be drawn is that this loading represents a reasonable approximation to the contact distribution.

This is in agreement with most contact solutions in which interface forces cluster towards the ends of the contact surface.

8. FILLET MODIFICATION

Since the small fillet radius in the critical region appeared to be a prime contributor to the stress concentration, a local geometry modification was undertaken as follows. The existing fillet radius (.055 in.) was systematically increased and the neighboring fillet at the bottom of the key-way was shifted without change in radius in order to maintain continuity of the boundary. Three different fillet radii were chosen. These three corresponded to multiples of 2, 3 and 4 times the original radius. This modification is best understood by looking at Figs. 14-17. A fourth modification consisted of replacing the two fillets and their connecting vertical boundary with the largest possible single circular arc which is tangent to both the 45° contact boundary and the horizontal boundary at the bottom of the keyway, without intruding into the contact area. This geometry is shown in Fig. 17, and is seen to be quite similar to Fig. 14.

The reference loading was applied to all four modified geometries. The resulting tensile stress distribution in their respective critical areas is plotted for each geometry in Figs. 14-17. These figures also contain their respective SCF.

It is seen from these stress distributions that increasing the fillet radius results in a decrease in the stress concentration and a shifting of the critical area away from the contact surface. However, the improvement reaches its optimum in Fig. 15 (3XR), and the stress then starts to rise with increasing radius. The conclusion to be drawn from this analysis is that, as expected, the stress concentration can be decreased up to 27% by increasing the fillet radius to an optimum value.

9. CONCLUSIONS

On the basis of a two dimensional parametric finite element simulation, the following conclusions can be drawn about the value and distribution of the edge tensile stresses in the critical contact/fillet area of the TF-30 third-stage turbine disk.

1. A likely interface condition consists of very little force at the center, with approximately twice as much force at the lug-fillet (inboard) end as at the other end.

2. The stress concentration factor (SCF) in the lug fillet for the most likely interface distribution and for a friction coefficient of .175 is 5.3.

3. The worst case SCF is 6.0.

4. Decreasing the coefficient of friction decreases the SCF.

5. Increasing the fillet radius can decrease the SCF by up to 27%.

6. In all cases the point of maximum SCF occurs farther into the fillet (away from contact area) than the point at which cracks have been observed to start.

7. The location of maximum SCF and general distribution are consistent with the experimental results of NRL Report 8149.

As a final graphical conclusion the shear and isopachic stress contours for the most likely loading are shown in Fig. 18, and linear plots of the tensile stress around the fillet and along the direction of observed fracture are shown in Fig. 19. It should be noted, from comparison of Figs. 18a b and Figs. 8 and 9, that the "most likely" interface loading does produce a shear stress pattern which is closer to the experimental pattern than any other distribution studied.

APPENDIX

NON-CENTRIFUGAL LOADING

During an oral presentation of the basic results on 14 February 1977, discussions with NAVAIR and Pratt and Whitney representatives indicated that they observed cracking to originate from a point inside the blade/disk-lug contact region, or removed from the point of maximum tensile edge stress as determined numerically and experimentally. Subsequent examination of the full disk/blade assembly provided to NRL showed the following: (1) 14 cracks originating from just inside the bearing area, all in lugs on the same side of their respective blades; (2) 2 cracks originating just outside the contact area (just into the fillet area), both in lugs on the side of the blade opposite to the other fourteen. This type of consistent unsymmetric behavior seemed to indicate a sensitivity to non-radial blade forces (assumed smaller) which might be superimposed on the centrifugal forces. This situation led to the following brief consideration of the effect of non-radial forces as they might cause a consistent lack of symmetry in the tensile edge stresses, relative to the discrepancy between locations of maximum stress and crack origination. Since the approach used in choosing possible perturbations in interface loading caused by non-radial blade loading involved a considerable amount of conjecture, the results should be interpreted in this context.

The initial analysis was based on an assumed centrifugal (radial) loading due to rotation of the disk. However there is also a wind force component perpendicular to the blade axis which tends to cock the blade to one side. It is evident that this cocking action will shift the contact forces towards opposite ends of the intended contact surface on either side of the blade. On one surface this cocking will tend to drive the distribution from the "most likely" situation (loading case NLIK + SLIK, Fig. 12) towards a more balanced distribution (loading case NDBT + SDBT). This increases the SCF less than 2%, but does not appreciably effect its location. On the other surface the contact forces will be driven towards the lug fillet, approaching a concentrated force condition (loading case (NCB + SCB). Rather than using a concentrated force to represent this situation, three new loadings were applied to the lug, each with normal and shear (17.5%) resultants equal to the reference loading. (The "most likely" loading is given as a reference in Fig. 20a, and the resulting tensile stresses in Fig. 20e.)

The first involved a linear variation from zero at the center of the contact area to a maximum at the end nearest the fillet, and no load on the other half of the interface (Fig. 20b). The second consisted of applying the full load at the two nodes nearest the fillet, with the closest node getting twice as much force as the next one. (Fig. 20c). The third consisted of shifting the two loading points of case two, each one node away from the fillet, leaving the closest node unloaded. (Fig. 20d). This last loading case is intended to study the effect of a small shift of the contact area away from the fillet area. Plots of the tensile stresses in the fillet/contact region for these three loading conditions are shown in Figs. 20f, 20g, and 20h. It is seen that there is no significant change in the value or location of the maximum tensile stress in relation to the reference loading case. However, Fig. 20g shows that shifting the contact area towards the fillet induces higher tensile stresses into the lower region of the contact area. This would result in a greater likelihood of cracks progressing from the lower end of the contact surface due to the presence of local imperfections. This is in accord with observations of a cracked disc in which all cracks which did not initiate in the fillet area occurred on the contact surface for which the blade-cocking tends to shift the contact towards the fillet region.

REFERENCES

1. V. J. Parks and R. J. Sanford, "Experimental Stress Analysis of the TF-30 Turbine Engine Third-Stage Fan-Blade/Disk Dovetail Region," NRL Report 8149, 1977.

2. L. A. Beaubien, "TOTAL: Interactive Graphics System For The Two-Dimensional Analysis of Linear Elastic Solids," Structural Mechanics Software Series, Vol. 1, University Press of Virginia, Charlottesville, Va., 1977.

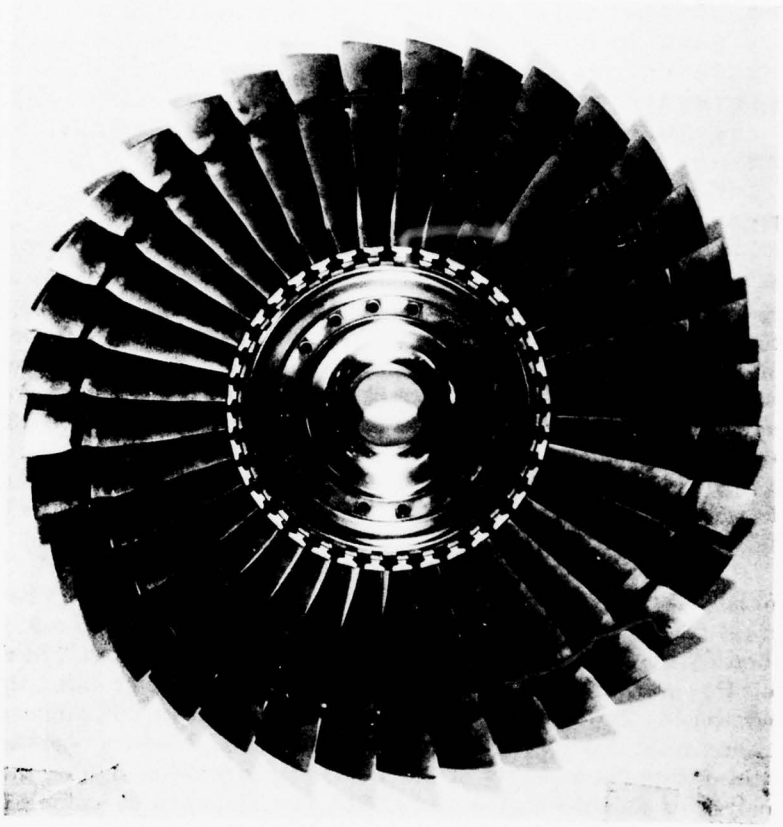

(a) Assembled third stage fan section

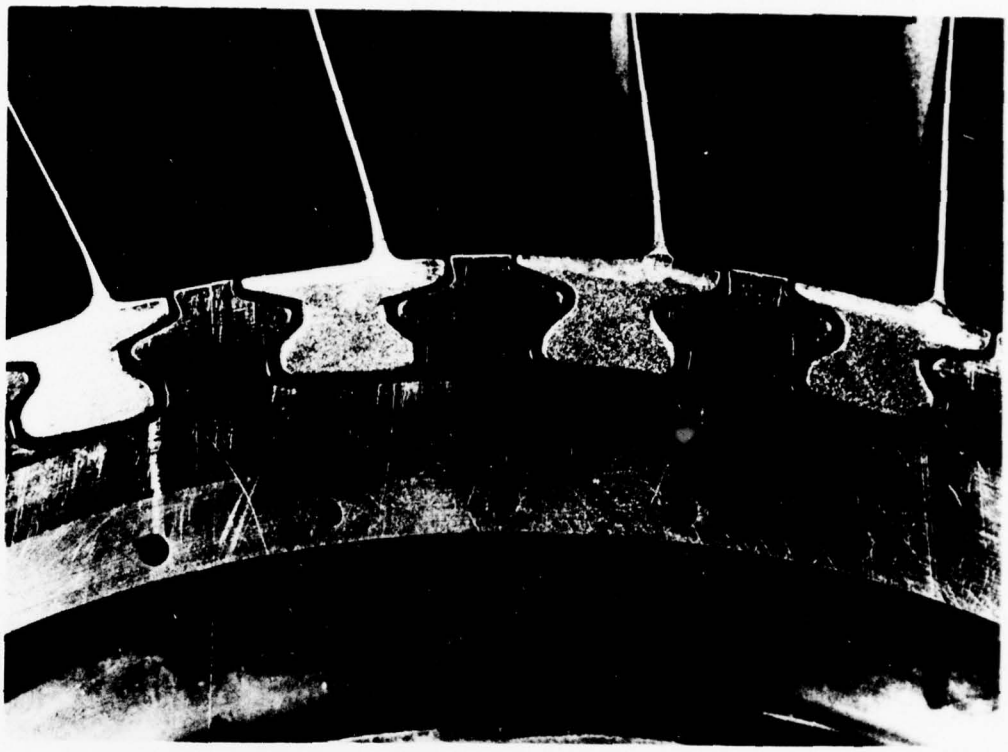

(b) Dovetail region

Fig. 1 — TF-30 third-stage disk/blade assembly

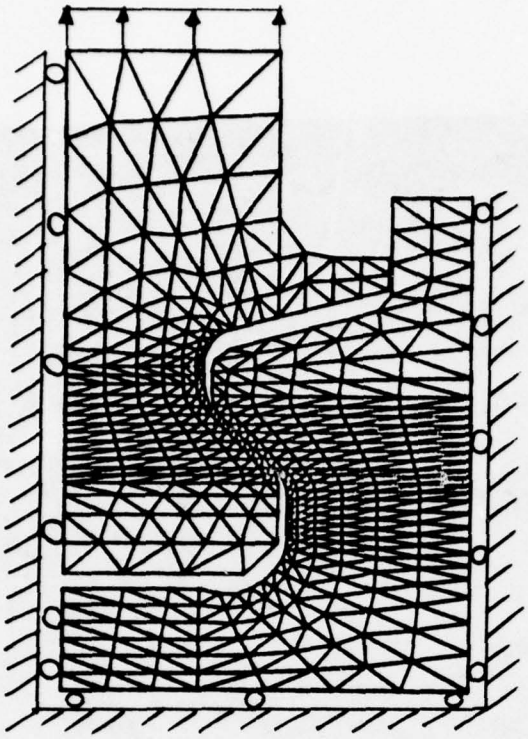

(a) Assumed physical loading

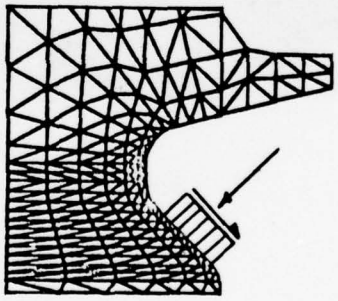

(b) Assumed interface loading
(reference loading)

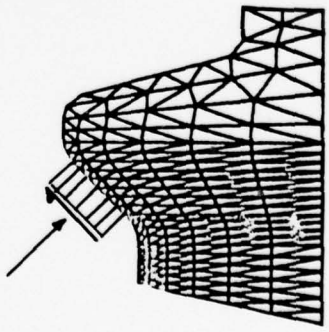

Fig. 2 — Simulated region with basic loads and constraints

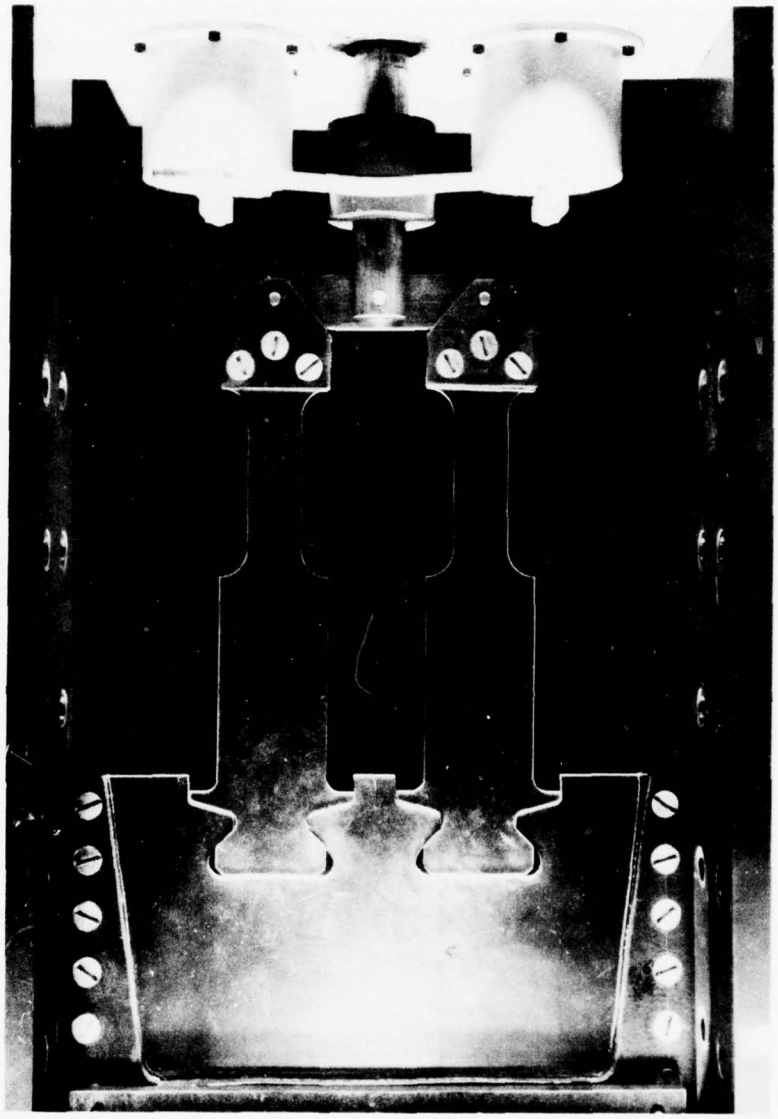

Fig. 3 — Experimental setup

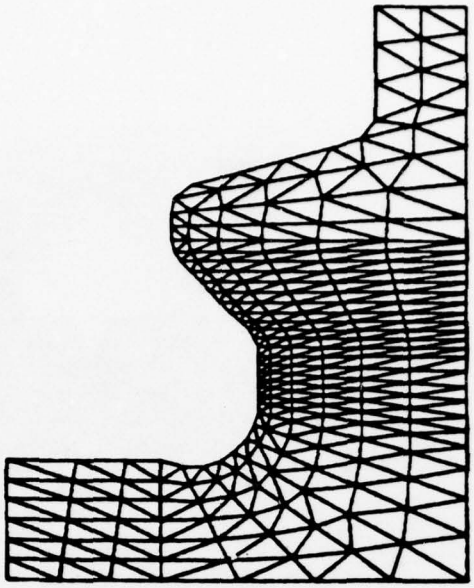

(a) Preliminary mesh

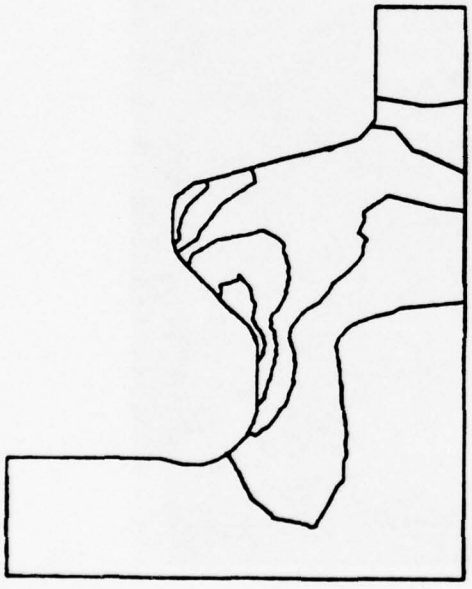

(b) Shear stress contours

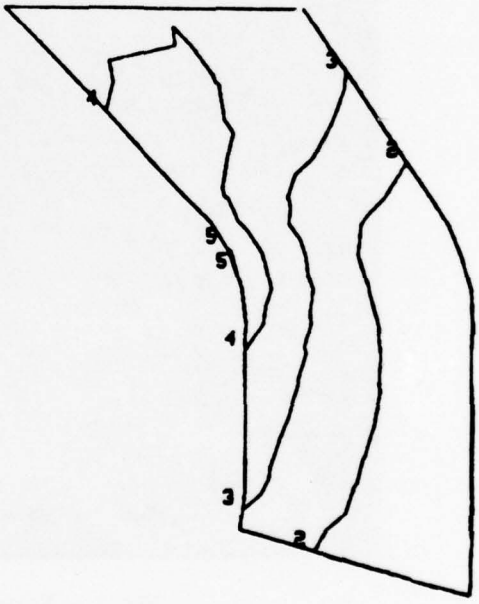

(c) Numbered local contours

Fig. 4 — Preliminary lug model evaluation

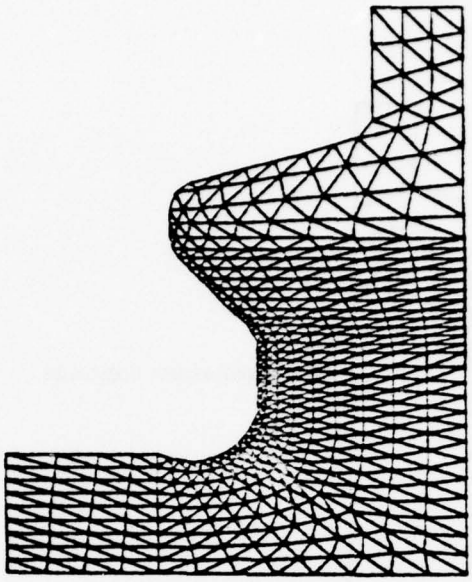

(a) Refined mesh

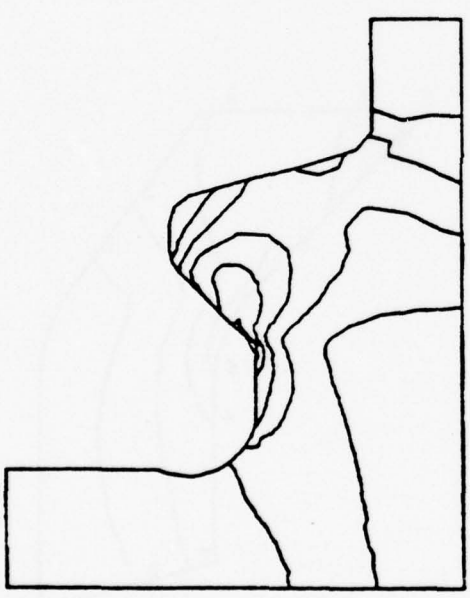

(b) Shear stress contours

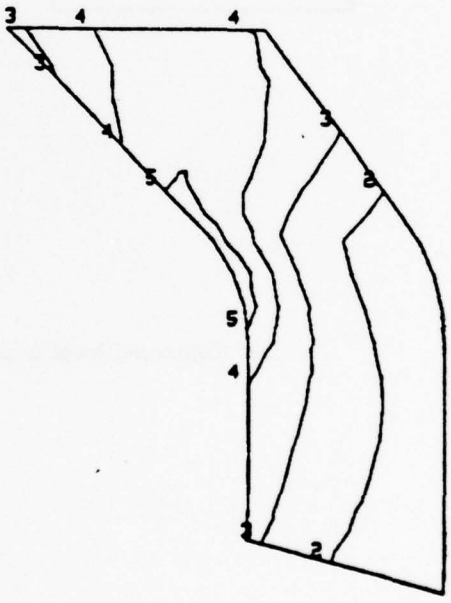

(c) Numbered local contours

Fig. 5 — Refined lug model evaluation

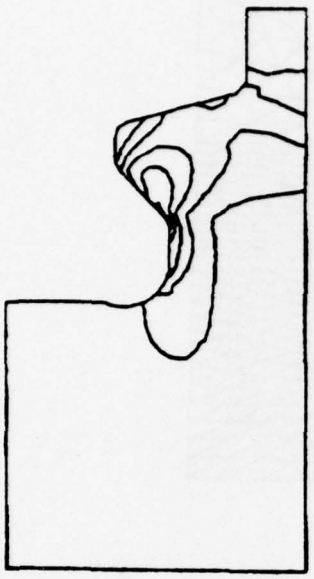

(a) Shear stress contours

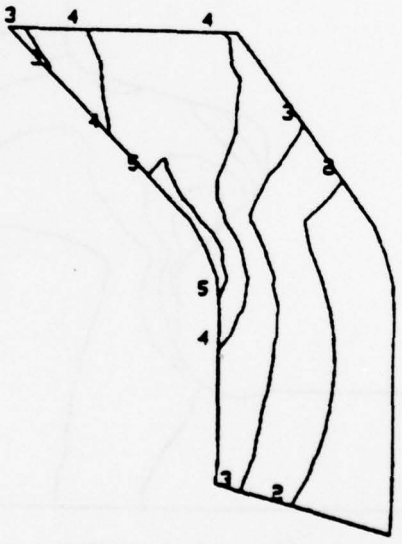

(b) Numbered local contours

Fig. 6 — Extended base model

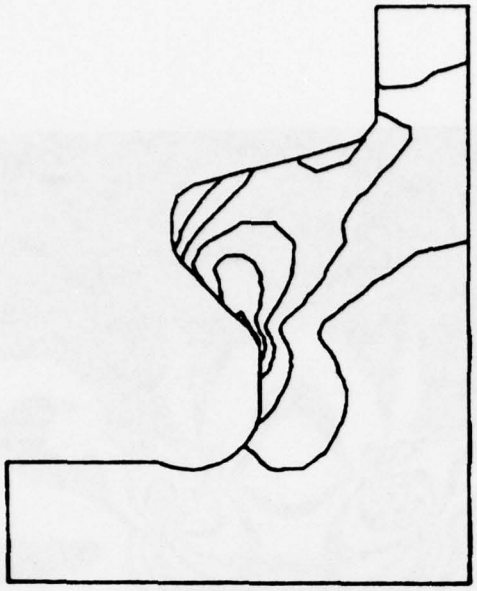

(a) Mesh with constraints

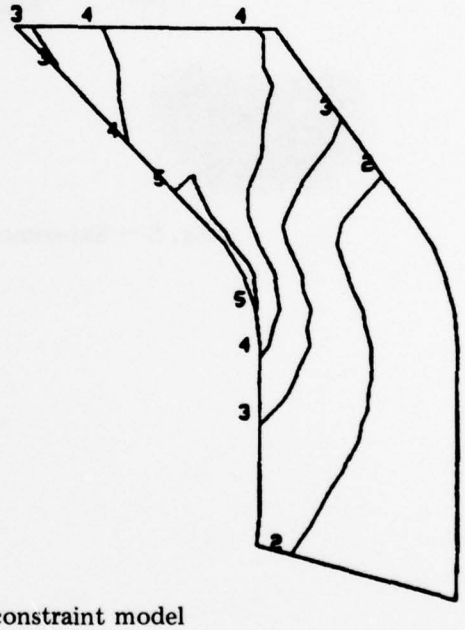

(b) Numbered local shear contours

Fig. 7 — Full edge constraint model

Fig. 8 — Experimental isochromatic contours

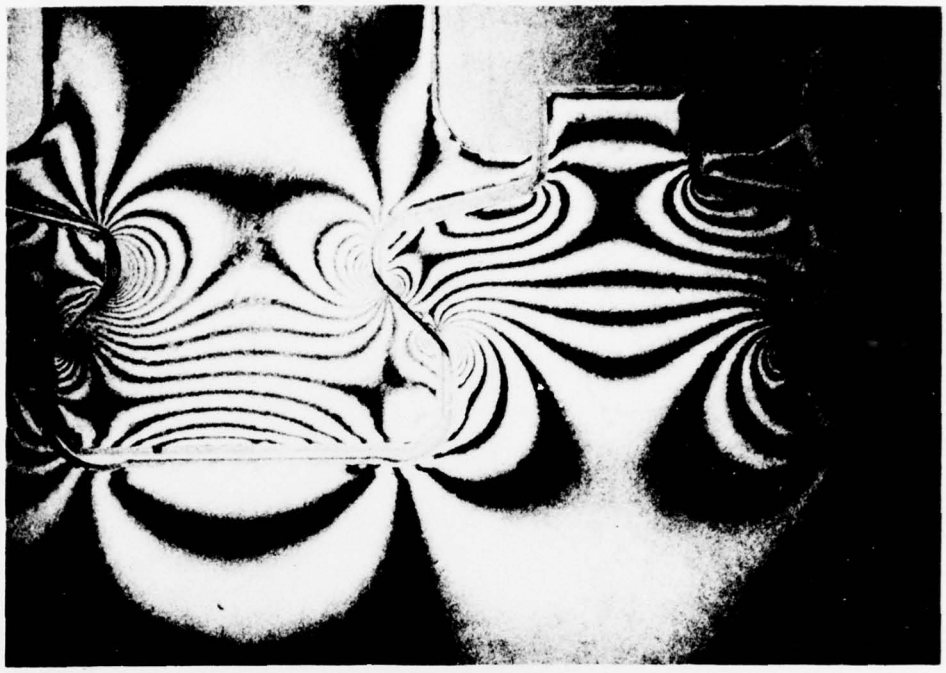

Fig. 9 — Experimental isopachic contours

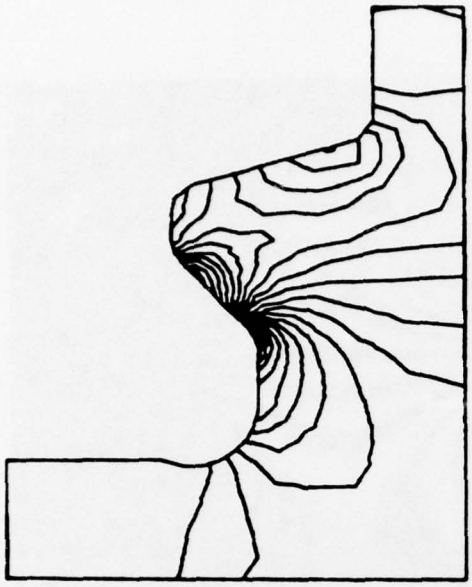

(a) Preliminary mesh

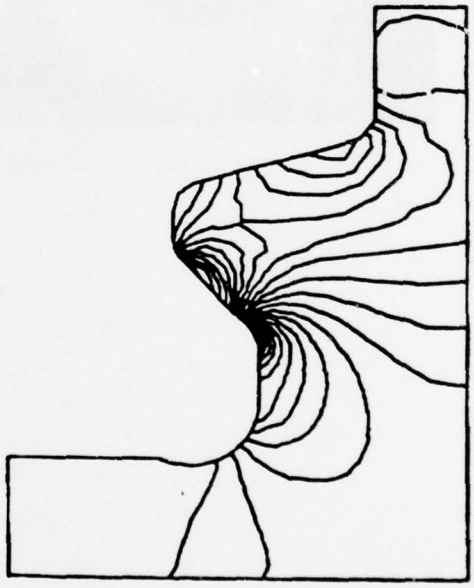

(b) Refined mesh

Fig. 10 — Numerical isopachic ($\sigma_1 + \sigma_2$) contours

(a) Full pattern

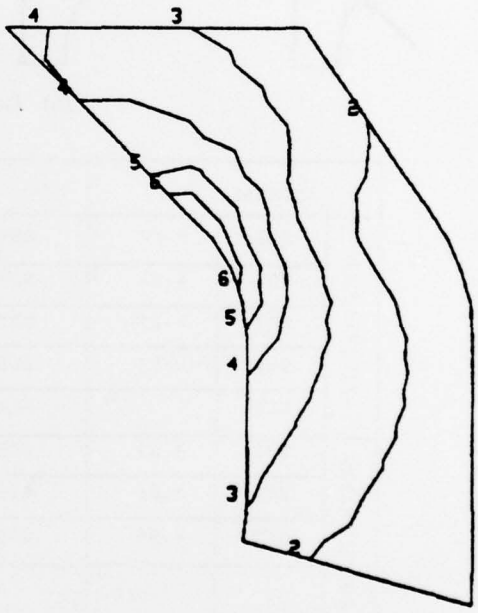

(b) Local detail

Fig. 11 — Shear stress (isochromatic) contours for linked (welded) condition

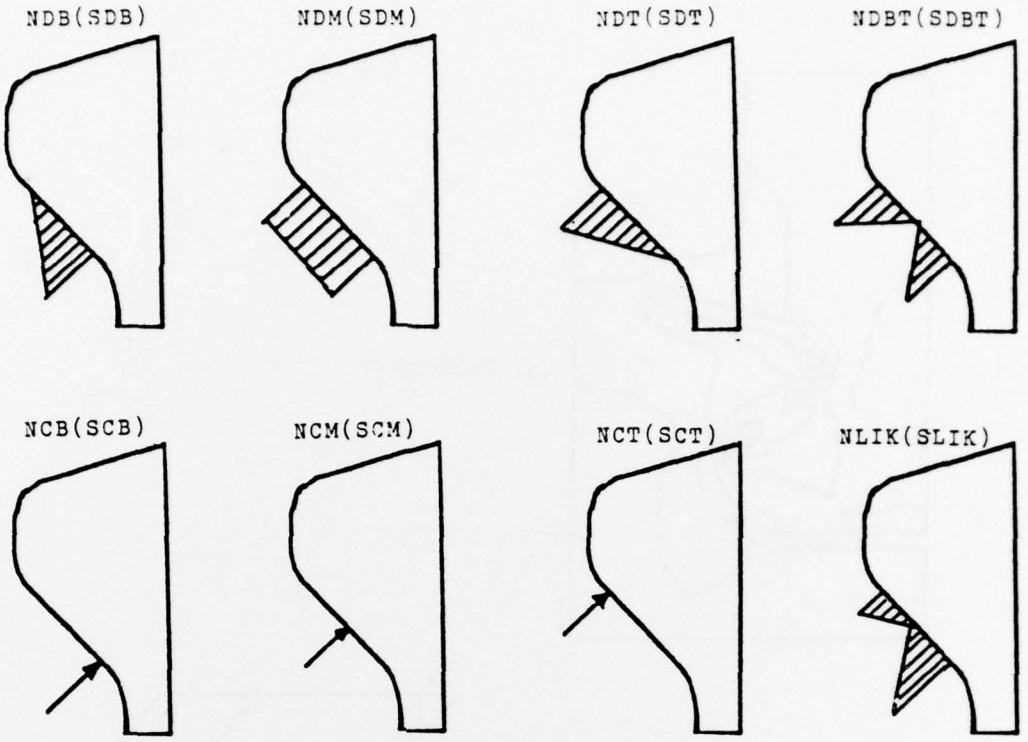

(a) Loading cases

	NORMAL		SHEAR		SUM
DISTRIBUTED	NDB	3.82	SDB	1.27	5.09
	NDM	4.04	SDM	1.20	5.24
	NDT	4.25	SDT	1.13	5.38
	NDBT	4.13	SDBT	1.24	5.37
	NLIK		SLIK		5.3
CONCENTRATED	NCB	3.89	SCB	1.66	5.55
	NCM	3.86	SCM	1.13	4.99
	NCT	4.96	SCT	1.09	6.05

(b) SCF (stress concentration factor) table

Fig. 12 — Loadings and resulting stresses

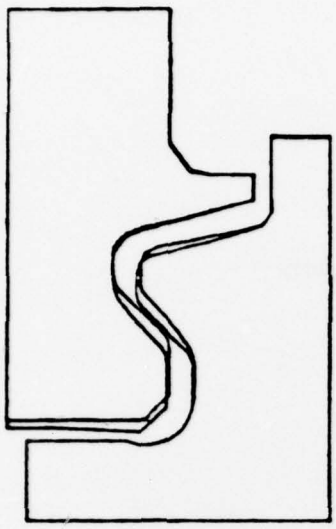

(a) Loading NDM + SDM

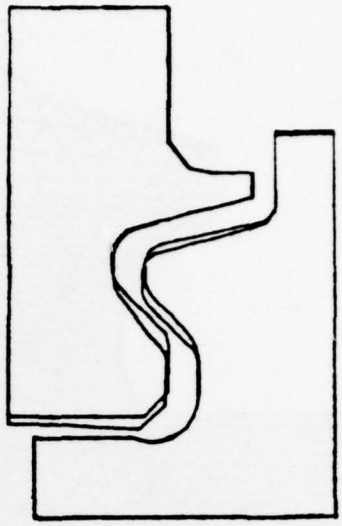

(b) Loading NDB + SDB

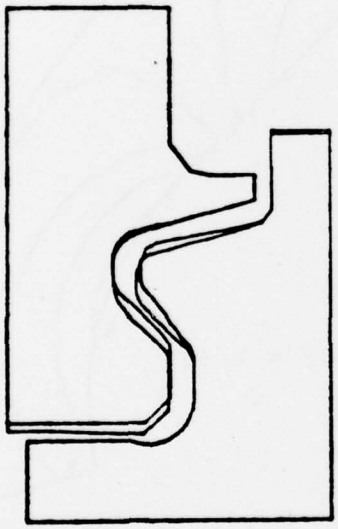

(c) Loading NDT + SDT

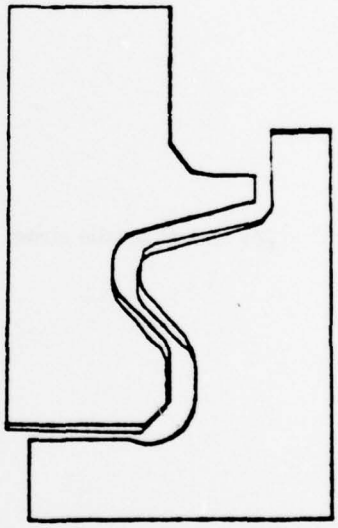

(d) Most likely loading NLIK + SLIK

Fig. 13 — Matching of interface displacements

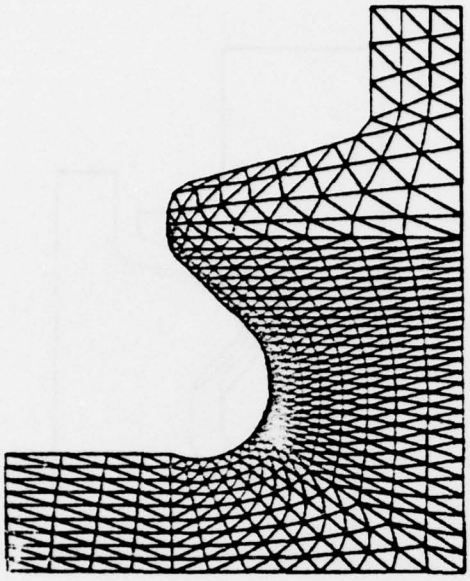

(a) Geometry

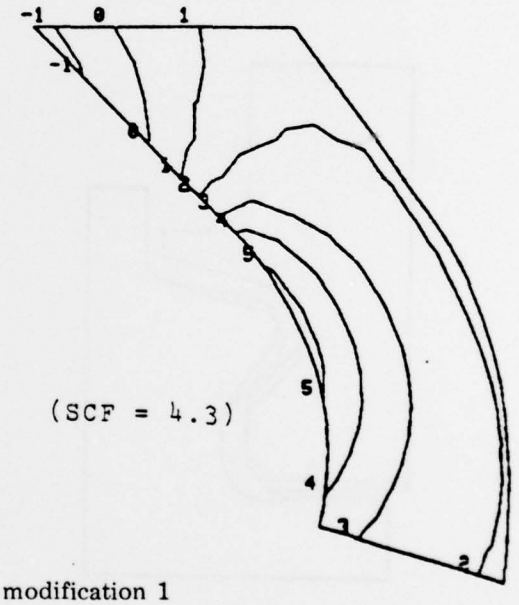

(b) Local tensile stress contours

Fig. 14 — Fillet modification 1

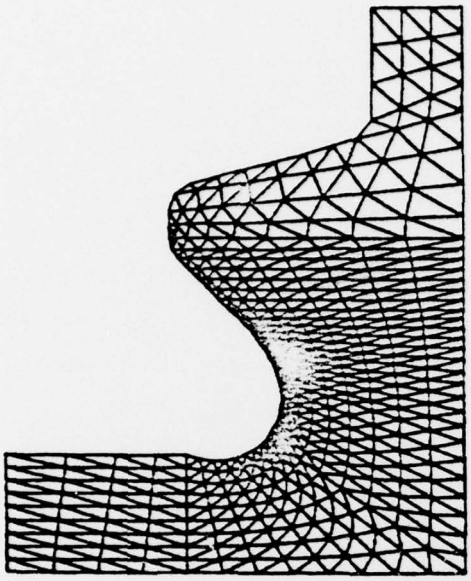

(a) Geometry

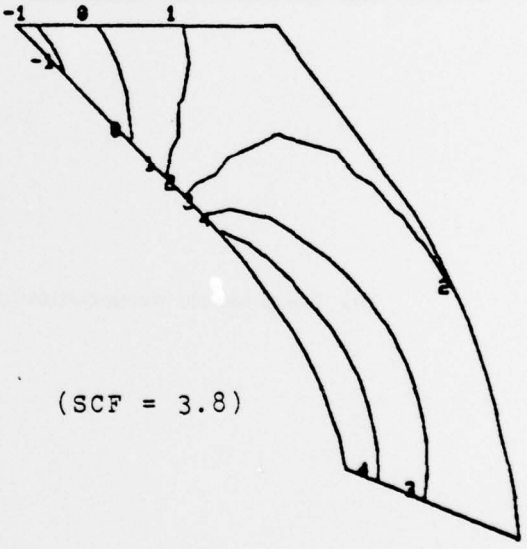

(b) Local tensile stress contours

Fig. 15 — Fillet modification 2

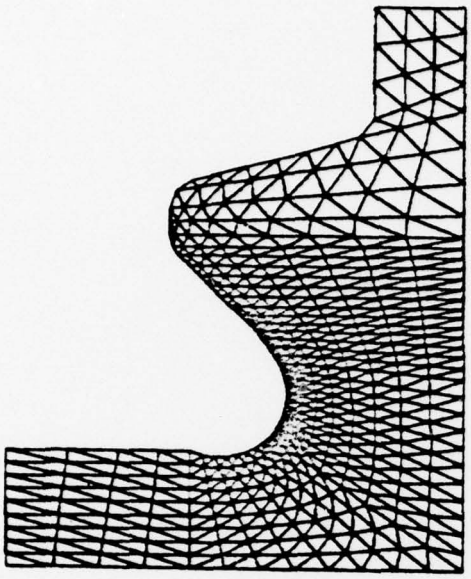

(a) Geometry

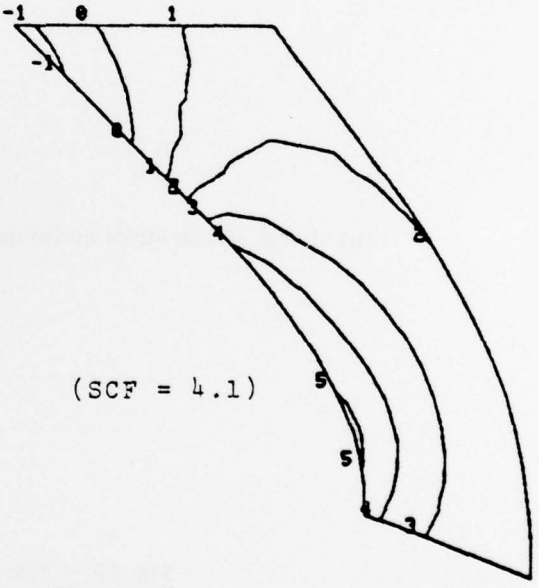

(b) Local tensile stress contours

Fig. 16 — Fillet modification 3

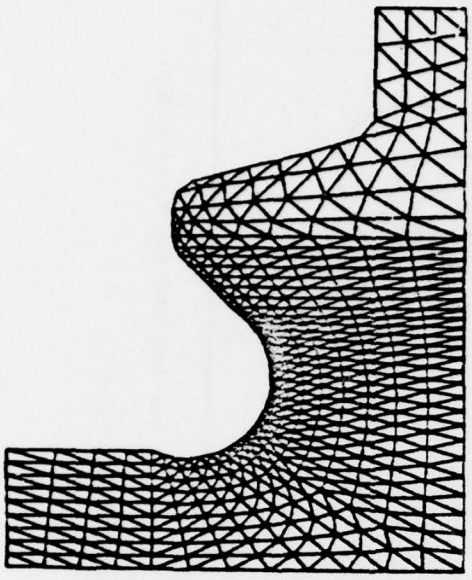

(a) Geometry

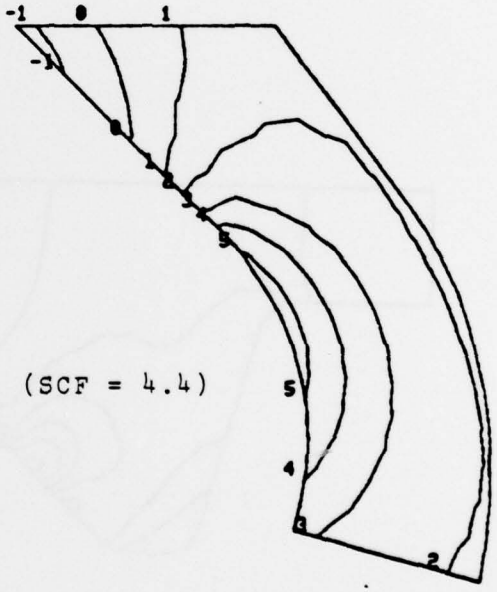

(b) Local tensile stress contours

(SCF = 4.4)

Fig. 17 — Fillet modification 4

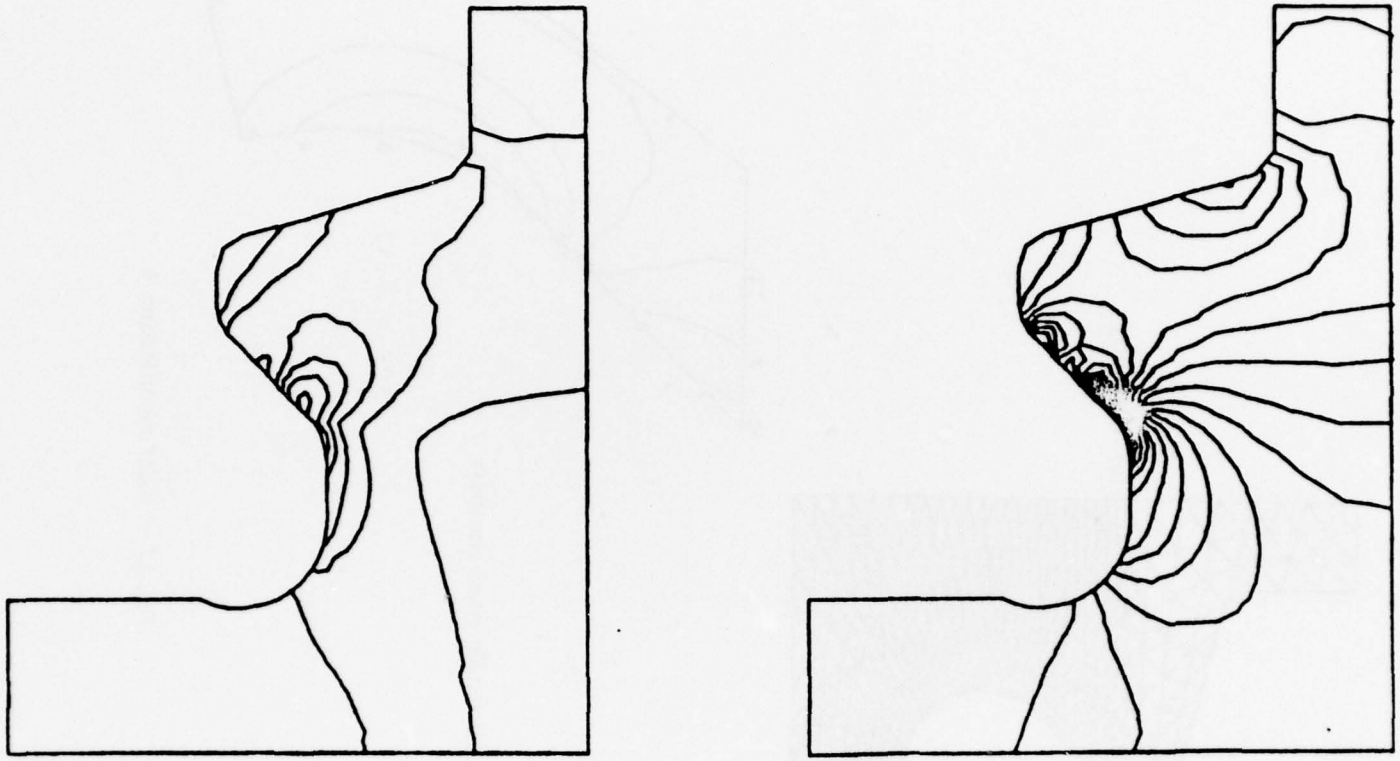

(a) Isochromatic (shear stress) pattern

(b) Isopachic ($\sigma_1 + \sigma_2$) pattern

Fig. 18 — Stress contours for most likely loading

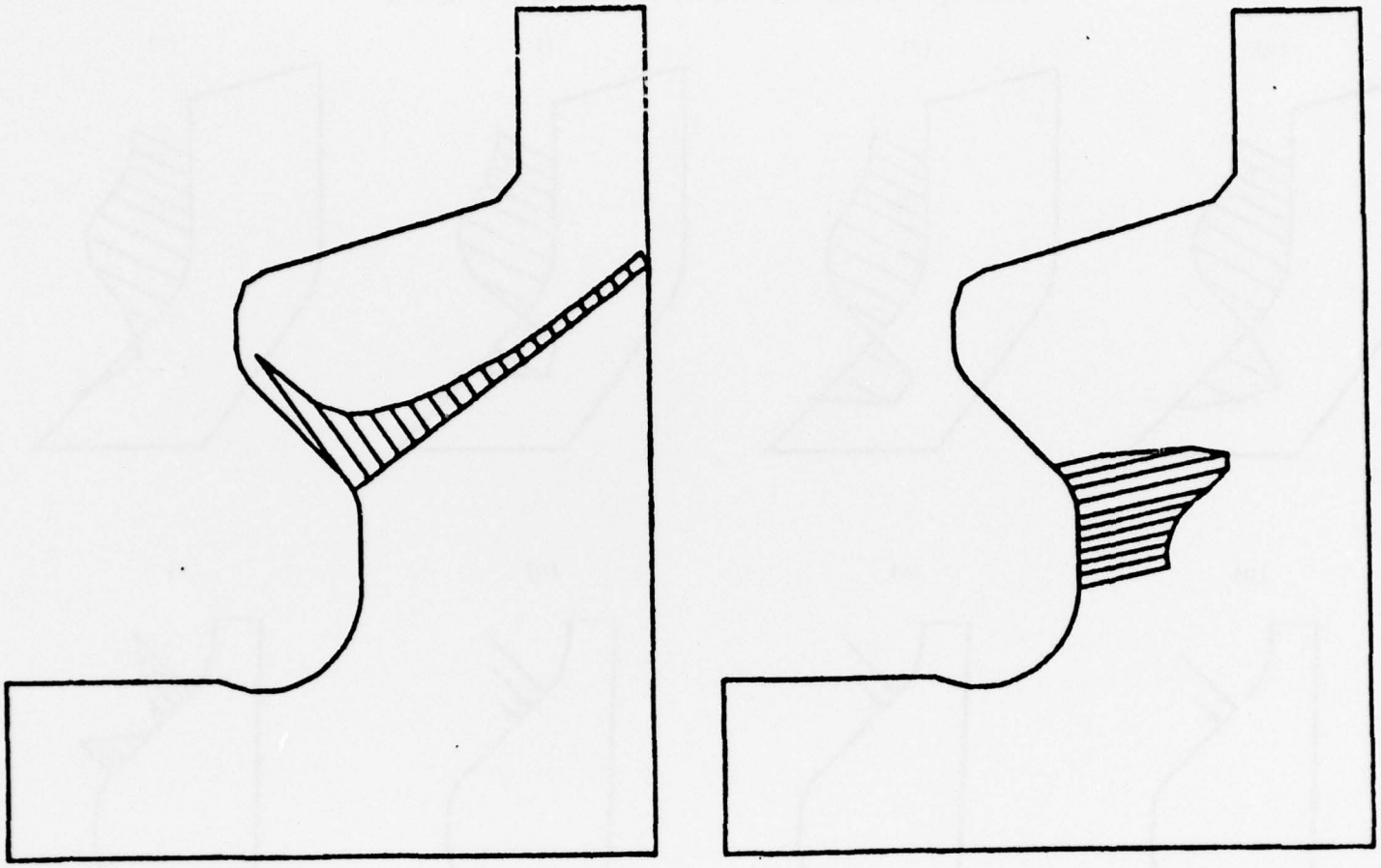

(a) Variation along observed fracture path

(b) Variation along contact/fillet edge

Fig. 19 — Linear tensile stress plots for most likely loading

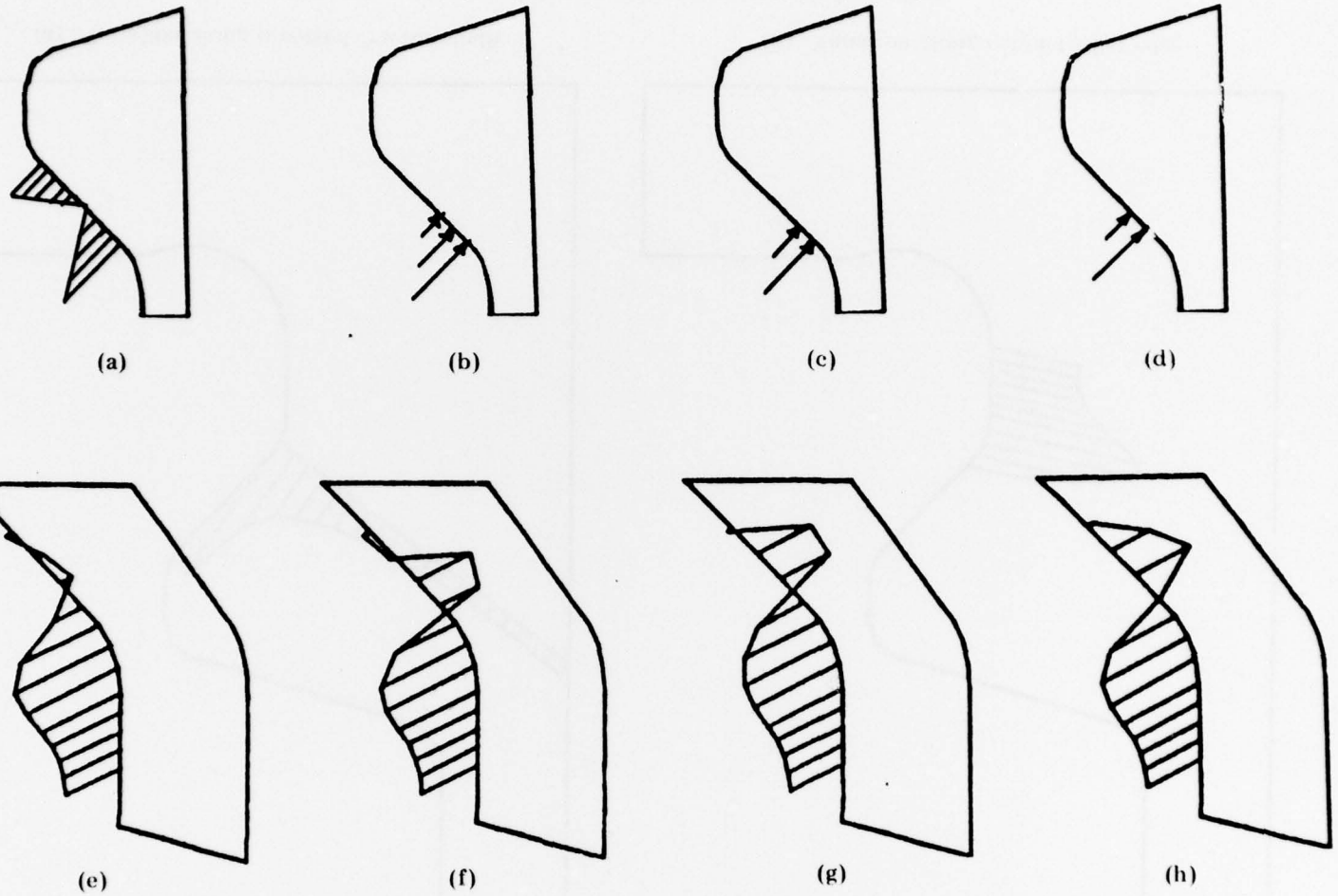

Fig. 20 – Unsymmetrical loads and resulting tensile stresses

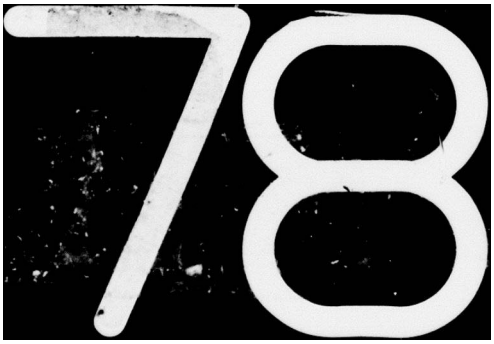
78